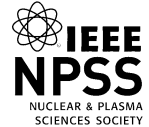


# IEEE TRANSACTIONS ON PLASMA SCIENCE



A PUBLICATION OF THE IEEE NUCLEAR AND PLASMA SCIENCES SOCIETY

SEPTEMBER 2020

VOLUME 48

NUMBER 9

ITPSBD

(ISSN 0093-3813)

---

REGULAR PAPERS

**Basic Processes in Fully and Partially Ionized Plasmas**

- Semianalytical Solution for Determination of Wave Amplification Characteristics in a Complex Elliptical Dielectric Waveguide Including Strongly Magnetized Plasma Circular Column ..... *Z. Rahmani and E. Heidari-Semiromi* 2961
- Experimental Determination of Threshold Powers for the Onset of HF-Enhanced Plasma Lines and Artificial Ionization in the Lower *F*-Region Ionosphere ..... *B. J. Watkins and S. P. Kuo* 2971
- Acceleration of Plasma Bullets by Grooved Dielectric Rod ..... *F. Sohbatzadeh, R. Ebrahimnezhad Darzi, and S. Mirzanejhad* 2977
- A Numerical Investigation on the Behavior of Electrons in the Bullet in the Atmospheric-Pressure Argon Plasma Jet ..... *C. Lu, Z. Tan, X. Chen, W. Lin, and X. Wang* 2987
- Parallel Propagating Waves in Weakly Magnetized Relativistic Electron Plasma ..... *W. Khan, M. Ali, and Y. Habib* 2996

**Microwave Generation and Microwave-Plasma Interaction**

- A Novel Method for Backward Wave Cancellation of Traveling Wave Tube Amplifier Using Ferrite Material ..... *M. Ghiasi, E. Hamidi, and F. Hodjat Kashani* 3001
- GYROCOMPU: Toolbox Designed for the Analysis of Gyrotron Resonators ..... *P. Wang, X. Chen, H. Xiao, O. Dumbrajs, X. Qi, and L. Li* 3007
- Analysis of the Combined Cyclotron and Cherenkov Resonances in Metallic Grating Structures ..... *X. Li, D. Zhao, Q. Xue, and Y. Xiang* 3017
- Cold Circuit Analysis of a Coupled-Cavity Slow Wave Structure for Mm-Wave TWT ..... *M. Sumathy, S. K. Gupta, B. Kumar, Y. Venkateswarlu, C. N. Murthy, M. Santra, and S. U. M. Reddy* 3024
- Analysis of Azimuthal Partition Periodic Disk-Loaded Coaxial Structure for Bifrequency MILO Using Equivalent Circuit Approach ..... *A. Kumar, P. Tripathi, S. Dwivedi, and P. K. Jain* 3030
- A 3-D Frequency-Domain Nonlinear Theory of the BWO With an Inclined Rectangular Electron Beam ..... *F. Zhang, Z. Zhang, D. Gao, and X. Wang* 3040
- Simulation of Multimode Competition of a Coaxial Cavity Gyrotron With Multiple Electron Beams ..... *S. Hou* 3047
- Plasma Diagnosis and Biomedical Application Using Linear Microwave Atmospheric-Pressure Plasma Generator ... *I. S. Eom, H. Y. Kang, and S. K. Kwon* 3054
- A Novel Leaky Wave Endfire Filtering Antenna Based on Spoof Surface Plasmon Polaritons ..... *W. Feng, Y. Feng, L.-S. Wu, Y. Shi, X. Y. Zhou, and W. Che* 3061

---

(Contents Continued on Page 2959)



---

An Ultraminiaturized Bandpass Filtering Marchand Balun Chip With Spiral Coupled Lines Based on GaAs Integrated Passive Device Technology .....	<i>Y. Yang, Y. Wu, Z. Zhuang, M. Kong, W. Wang, and C. Wang</i>	3067
Design and Simulation of an S-Band Relativistic Inverted Magnetron .....	<i>T. P. Fleming</i>	3076
Application of Map-Based Multipactor Theory to Alternate Periodic Radio Frequency Waveforms .....	<i>M. Siddiqi</i>	3083
<b>Charged Particle Beams and Sources</b>		
Effect of Laser Polarization Mode on Wake Wave Excitation in Magnetized Plasma ...	<i>Y. Heydarzadeh and H. Akou</i>	3088
A Novel Technique for Optimizing 270°-Bent Electron Gun for Evaporation Applications .....	<i>V. Goel, A. Roy, and N. Maiti</i>	3098
Thermal Electron Flow in a Planar Crossed-Field Diode .....	<i>D. Chernin, A. Jassem, and Y.Y. Lau</i>	3109
<b>Industrial, Commercial, and Medical Applications of Plasmas</b>		
Evaluation of DBD Plasma Effects on Barley Seed Germination and Seedling Growth .....	<i>A. Mazandarani, S. Goudarzi, H. Ghafoorifard, and A. Eskandari</i>	3115
Computation of Optimal Operation Voltage of the Neon-Filled Plasma Pockels Cell .....	<i>E. I. Bochkov, L. P. Babich, S. A. Bel'kov, and Y. V. Dolgoplov</i>	3122
Effect of the Electrode Material on Ignition of Ethylene–Air Mixtures .....	<i>A. Reguig, J. S. Damazo, E. Kwon, and D. A. Lacoste</i>	3128
<b>Plasma Diagnostics</b>		
Tomographic Reconstruction of the Neutron Time–Energy Spectrum From a Dense Plasma Focus .....	<i>J. Catenacci, D. Constantino, B. Gall, and A. Luttmann</i>	3135
Dual-Wavelength Interferometric Measurement of Electrically Exploded Aluminum and Copper Wires in Low-Pressure Air for Electron and Ion Density Calculation .....	<i>A. Hamilton, M. A. Saville, and V. Sotnikov</i>	3144
Heat Flux Analysis From IR Imaging on Proto-MPEX .....	<i>C. Lau, J. F. Caneses, P. A. Piotrowicz, M. A. Showers, C. J. Beers, T. M. Biewer, T. S. Bigelow, J. B. O. Caughman, R. H. Goulding, N. Kafle, and J. Rapp</i>	3152
Dynamics of the Effluent Gas Turbulent Front of the Plasma Jet Driven by Dual Sources of a Pulsed DC and AC Power: Experimental Study .....	<i>M. Ghasemi, S. Yu, and M. H. Qaisrani</i>	3160
<b>Pulsed Power Science and Technology</b>		
Study on the Basic Characteristics of Solid-State Linear Transformer Drivers .....	<i>J. Rao, Y. Zhu, Y. Wang, S. Jiang, and Z. Li</i>	3168
A New High-Efficiency Power Management Circuit for a Novel Two-Phase Compensated Pulse Alternator .....	<i>B.-S. Nguyen, W.-W. Yen, P. C.-P. Chao, and S.-C. Wang</i>	3176
Solid-State Linear Transformer Driver Using Inductive Energy Storage .....	<i>Y. Feng, T. Sugai, A. Tokuchi, and W. Jiang</i>	3188
<b>Arcs &amp; MHD</b>		
Determination of the Electrical Circuit Equivalent to a Pulsed Discharge in Water: Assessment of the Temporal Evolution of Electron Density and Temperature .....	<i>T. Merciris, F. Valensi, and A. Hamdan</i>	3193
<b>Electromagnetic Launch Science and Technology</b>		
Design and Implementation of a High-Speed Real-Time Position Detection System in Electromagnetic Coil Launcher .....	<i>G. X. Cun, S. Wang, D. Guo, S. Guan, B. Liu, and B. Wu</i>	3203
Coupling Analysis and Research of Multistage SICL Based on Crowbar Circuit .....	<i>S. Guan, D. Wang, X. Guan, W. Li, T. Gao, and L. Qiu</i>	3211
A Hybrid Simulation Model for Electromagnetic Launchers Including the Transient Inductance and Electromotive Force .....	<i>N. Tosun, H. Polat, D. Ceylan, M. Karagöz, B. Yıldırım, İ. Güngen, and O. Keysan</i>	3220
<b>Terahertz Science &amp; Technology</b>		
0.2-THz Traveling Wave Tube Based on the Sheet Beam and a Novel Staggered Double Corrugated Waveguide ....	<i>Z. Lu, W. Ge, R. Wen, Z. Wang, H. Gong, Y. Wei, and Y. Gong</i>	3229
Application of a Compact Sub-Terahertz Gyrotron for Nondestructive Inspections .....	<i>S.-T. Han</i>	3238
A Multifrequency Electromagnetic Modulator Based on the Solid-State Plasma Metamaterial .....	<i>G.-B. Liu and H. Zhang</i>	3246
<b>Other Topics in Plasma Science</b>		
Amplification of Propagating Spoof Surface Plasmon Polaritons in Ring Resonator-Based Filtering Structure .....	<i>R. K. Jaiswal, N. Pandit, and N. P. Pathak</i>	3253

---

(Contents Continued from Page 2959)

---

Temporal and Spectral Characterization of Electromagnetic Pulse Emitted From Nanosecond Pulsed Laser Produced Aluminum Plasma .....	<i>S. Ullah, H. Qayyum, Z. U. Rehman, A. H. Dogar, and A. Qayyum</i>	3261
<b>Special Issue - Selected Papers from SOFE 2017</b>		
Endoscope Emulator Test Bench for ITER Dust Monitor Diagnostic .....	<i>E. Veshchev, Y. Sadovskiy, L. Begrambekov, O. Bidlevitch, O. Gordeev, P. Shigin, G. Vayakis, M. Walsh, and R. Walton</i>	3267
<hr/>		
COMMENTS AND CORRECTIONS		
Comment on “Growth of Low-Frequency Electrostatic and Electromagnetic Instabilities in a Hall Thruster” by Singh and Malik (2011) .....	<i>Y. Elskens and N. Lemoine</i>	3272
<hr/>		
ERRATA		
Erratum to “Transfer Learning as a Tool for Reducing Simulation Bias: Application to Inertial Confinement Fusion” .....	<i>B. Kustowski, J. A. Gaffney, B. K. Spears, G. J. Anderson, J. J. Thiagarajan, and R. Anirudh</i>	3275

---

# Experimental Determination of Threshold Powers for the Onset of HF-Enhanced Plasma Lines and Artificial Ionization in the Lower $F$ -Region Ionosphere

Brenton J. Watkins<sup>1</sup>, *Member, IEEE*, and Spencer P. Kuo<sup>2</sup>, *Fellow, IEEE*

**Abstract**—HF heating experiment, with linear power ramp from 50 to 92 dBW, was conducted to determine the HF threshold power levels for the onset of detectable plasma waves and the onset of artificial ionization inferred from HF-enhanced plasma lines (HFPLs). The threshold free-space electric field at 200-km altitude, where HFPLs were detected, is about 53 mV/m. However, the HF electric field near the reflection height is enhanced by a swelling factor  $\sim 3.76$  and also conversion to a linear dipole pump mode ( $\sqrt{2}$ ); the actual threshold field is about 281 mV/m that is consistent with theory. Artificial ionization in the lower region was detectable via UHF radar. Short wavelength upper-hybrid waves, which were excited parametrically by the HF heating wave at higher threshold, implement Doppler shifted harmonic-cyclotron resonance interaction, via finite Larmor radius effect, to effectively accelerate electrons. Monitoring the spectral power of the parametric decay instability (PDI) line in the HFPLs by radar was shown to determine the artificial ionization onset time more precisely than that by observing the start of a sharp downward trend in the altitude of the HFPLs; at this time, the HF free-space electric field slightly below 200-km altitude is about 550 mV/m. Langmuir cascade lines in the HFPLs are separated by intervals about double the ion-acoustic frequency (about 4–5 kHz) generated by the PDI. These lines, observed at lower power facilities, were not observed. The upper-hybrid OTSI and PDI excited at HighPower Active Auroral Research Program (HAARP) and the mode competition nonlinear-damping mechanism are suggested as the processes, suppressing cascade enhanced HFPLs.

**Index Terms**—Artificial ionization, HighPower Active Auroral Research Program (HAARP), parametric decay instability (PDI), plasma line, upper-hybrid wave.

## I. INTRODUCTION

THE HighPower Active Auroral Research Program (HAARP) ionospheric modification facility at Gakona, Alaska was operated with a scheme to slowly increase the HF transmitted power from a very low level to full power

Manuscript received March 16, 2020; revised May 27, 2020; accepted July 27, 2020. Date of publication August 18, 2020; date of current version September 11, 2020. This work was supported by the High Frequency Active Auroral Research Program (HAARP). The work of Brenton J. Watkins was supported by the Defense Advanced Research Programs Agency (DARPA) Basic Research on Ionospheric Characteristics and Effects Program under Contract HR0011-09-C-0099. The review of this article was arranged by Senior Editor F. Taccogna. (*Corresponding author: Brenton J. Watkins.*)

Brenton J. Watkins is with the Geophysical Institute, University of Alaska Fairbanks, Fairbanks, AK 99775 USA (e-mail: watkins@usa.net).

Spencer P. Kuo is with the New York University Tandon School of Engineering, Brooklyn, NY 11201 USA (e-mail: spk259@nyu.edu).

Color versions of one or more of the figures in this article are available online at <http://ieeexplore.ieee.org>.

Digital Object Identifier 10.1109/TPS.2020.3014140

with the objective to investigate the onset threshold fields for parametric instability and artificial ionization in the  $F$ -region of the ionosphere. A UHF diagnostic radar [1] operating at 446 MHz was used to scatter from HF-enhanced plasma waves, and to infer the production of artificial ionization.

The HAARP facility uses a phased-array antenna composed of crossed dipoles in a  $12 \times 15$  array. The maximum power radiated is about 3.2–3.6 MW, depending on the particular HF frequency used, that covers a range of 2.8–9 MHz.

The UHF diagnostic radar operates with a relatively low peak pulse power (about 250 kW) and is not able to detect scatter from naturally occurring thermal fluctuations usually termed “incoherent-scatter.” In contrast, radar signals scattered from plasma waves enhanced by high-power HF waves from HAARP are quite strong, typically 3 dB or more above the radar receiver noise level with integration times about 0.5 s. An example of HF-enhanced ion-acoustic waves is shown by Oyama *et al.* [1] with low HF power before the HAARP facility was completed. Many similar radar observations made at Arecibo, EISCAT, and so on [2], [3] have also detected HF-enhanced ion-acoustic and Langmuir waves, demonstrating the role of the parametric decay instability (PDI) during HF ionospheric modification experiments. The completed HAARP system provides considerably greater maximum power compared with other facilities and a new phenomenon associated with artificial ionization was observed. The plasma response at the HAARP facility differs from observations at other facilities that operate at substantially lower power and this will be discussed in Section II.

In the present work, experiments were performed to study HF-enhanced ion-acoustic and Langmuir waves, and effects such as artificial optical emissions and ionization, instigated by the high-power HF waves transmitted from the HAARP ionospheric modification facility. A linear increase in transmitting HF wave with the effective isotropic radiated power (EIRP) varied from 50 to 92 dBW (100 kW to 1.6 GW) was used. Initially, at the beginning of the HF heater turn-on at low power levels, only four dipole antennas were utilized and as the transmitted power slowly increased, other transmitting dipoles were successively added to accomplish the linear power ramp. The HAARP antenna that transmitted the HF wave, and also the UHF diagnostic radar, was phased to orient the antenna beams along the magnetic zenith ( $AZ = 202$ ,  $EL = 76$ ).

This linear power ramp approach enables determination of the transmitted power levels for the onset of detectable plasma waves and the onset of artificial ionization [4], [5], inferred from the intensity variation and altitude shift of the HF enhanced plasma lines (HFPLs). The results can then be used to calculate the power densities and electric fields at 200-km altitude, near the altitude of the observed plasma waves, to justify the theoretical threshold field of the Langmuir PDI (L-PDI) [6], [7] and to provide essential data as the reference for the theoretical study of artificial ionization process [8].

In Section II, the experiment and procedure are described; the experimental results are also presented and discussed. Summary of the work in comparison with the theory is given in Section III.

## II. EXPERIMENT PROCEDURE AND RESULTS

The HAARP HF transmitter was operated for a 120-s period; it radiated in the magnetic zenith direction and the EIRP increased linearly from 50 to 92 dBW. The frequency  $f_0$  used was 5.760 MHz near the fourth electron gyro-harmonic frequency at about 200-km altitude where the HFPLs were observed with the diagnostic radar. A specific time during the HF power ramp is associated with an EIRP (in units of dBW) that can be converted to a free-space HF electric field at the altitude of interest. The EIRP value is obtained from engineering measurements of the total power radiated and the antenna gain. The procedure for calculating the electric field generated by the HAARP HF wave is as follows. The EIRP value provides an equivalent isotropic power flux per square meter ( $\text{W/m}^2$ ) that is radiated. This intensity varies with height with an inverse distance squared dependence; thus, the intensity may then be calculated for our height of interest (200 km). The total wave energy density is distributed between electric and magnetic fields and we then calculate the portion attributed to the electric field. This procedure has been outlined in many texts, for example, Davies [17]. The method was used for determining the threshold electric fields for both the initial observable occurrence of the L-PDI and the occurrence of artificial ionization.

The experiment procedure during the power ramp period was, therefore, to identify the specific times for the initial observable onset of plasma waves and the onset of artificial ionization, then the electric fields at those specific times were calculated and compared with theory.

Radar detection of plasma waves is limited to waves with near-field-aligned propagation, and other wave processes near-perpendicular to the earth's magnetic field are not detectable with colocated diagnostic radars. The UHF diagnostic radar was operated with a pulselength of 996  $\mu\text{s}$ , and a pulse repetition rate of 100 Hz, thereby maintaining the average power and duty cycle just below maximum allowed values. The pulse was phase-modulated with a 249-bit binary code with 4- $\mu\text{s}$  bauds, yielding 600-m range resolution after decoding. Complex voltage samples at all ranges were acquired and stored for every radar pulse and no on-line integration was performed. We have, therefore, been able to subsequently process data with varying integration times to suit particular

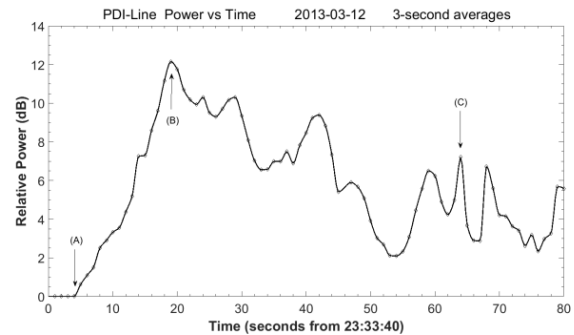


Fig. 1. Time dependence of the power of the down-going PDI line in the HFPLs. Three specific times are marked, (A) corresponds to the onset of detectable Langmuir waves associated with the PDI, (B) marks the end of the power increase, and (C) denotes the onset of artificial ionization.

experiments and data processing needs. We show results from power spectra derived for selected 600-m range intervals near the interaction altitude (about 200 km) of the high-power HF wave.

The UHF radar has only one receiving frequency channel and was set to continuously monitor the “up-shifted” plasma lines, i.e., plasma lines above the 446-MHz radar frequency. The receiver spectral bandwidth was 250 kHz that is offset in the frequency domain relative to the UHF transmit frequency where spectral analysis was performed to receive plasma-line signals from 5.730 to 5.770 MHz above 446-MHz radar frequency. The PDI line in the HFPLs is observable at about 5.755 MHz that is downshifted from 5.760 MHz (HAARP HF frequency) by the ion-acoustic frequency appropriate for the 446-MHz radar wavelength. The HFPLs that typically appear over two or sometimes three ranges (about 1.2–1.8 km) result from the parametric decay of the HF pump wave into a Langmuir sideband and ion-acoustic decay mode. During the 120-s duration of the HF power ramp, the total spectral power of this PDI line only with 300 pulse (3 s) moving average is plotted in Fig. 1, showing the relative spectral power variation during the HF power ramp period. Although the duration of the power ramp was 120 s (23:33:00–23:35:00 UT), for clarity, Fig. 1 shows only 80 s of data beginning at 23:33:40 UT because prior to this time, there were no detectable signals and this 80-s period includes the onset of detectable signals and also the onset of artificial ionization.

Ionograms acquired during the experiment period indicate that the ionosphere was stable with foF2 value about 7.5 MHz and peak  $F$ -region height about 240 km. The ionosonde data also indicate very minimal ionospheric absorption at HF frequencies because there was a persistent double-hop in the ionogram traces, i.e., the reflected wave propagates upward again after reflection from the ground.

Fig. 1 shows total power for the down-going PDI line in the HFPLs as a function of time (it excludes power in other HFPLs). This signal results from the L-PDI that occurs immediately below the HF reflection height (at  $f_{pe} = f_0 = 5.760$  MHz).

Relevant times (A), (B), and (C) are marked in Figs. 1 and 2. Fig. 2 shows the total relative power received by the diagnostic radar as function of time and range. The time marked (A)

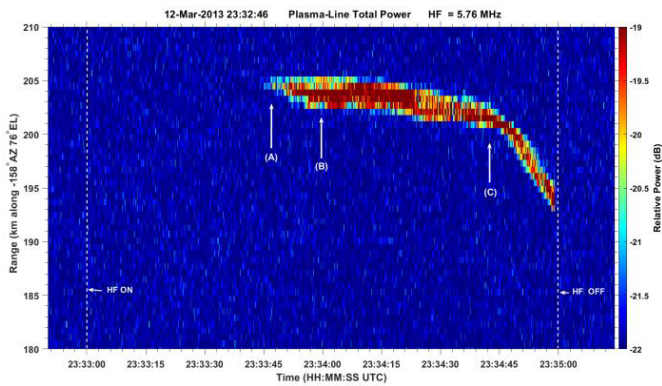


Fig. 2. Total down-going HFPL power as function of time. The times labeled (A), (B), and (C) correspond to the times in Fig. 1. The color scale is relative power in dB units. The decrease in altitude of the HFPLs after time (C) is interpreted to be the onset of artificial ionization.

corresponds to the time for the first detectable HFPL signals. The time (B) is the time of peak power in the HFPLs. The time marked (C) denotes the onset of artificial ionization when the height of the HFPLs (evident from Fig. 2) begins to drop.

The specific times for the onset of the L-PDI (time A in Fig. 1) and the onset of artificial ionization (time C in Fig. 1) are important because any errors will be reflected in the calculated electric field values. The 120-s linear power ramp (50–92 dBW) started to 23:30:00 UT. The EIRP in units of dBW at a given time was then calculated from  $EIRP = [(92 - 50)/120]t + 50$ , where  $t$  is units of seconds from 23:30:00 UT. For reasons of clarity, Fig. 1 shows only the final 80 s of the 120-s power ramp because no signals were seen before 23:33:45 UT that is marked time A in Fig. 1. To optimally establish this time, individual power spectra versus height, such as those shown in Fig. 4, were manually examined near this onset time. The diagnostic radar data were processed with 50 pulse averages, i.e., 500-ms time resolution. Next, the relative power from four range gates that encompassed the PDI line were manually summed. This was repeated for several 500-ms periods around the time A marked in Fig. 1. A very clear start time was established to be 23:33:45 UT, i.e.,  $t = 45.0$  s in the above equation to determine the  $EIRP = 65.75$  dBW with a subsequent calculation of 53 mV/m at 200-km height. Any possible uncertainty in selection of this time would not exceed 500 ms that translates to about 1 mV/m. The same procedure discussed later was used to determine the onset time for artificial ionization.

As the HF heating power exceeds the level at time (B), the overall spectral power of the down-going PDI line in the HFPLs starts to drop; but it is also evident that there are numerous variations in magnitude as the HF heating power is increased. We interpret the decreasing trend together with peaks in the variations of the spectral intensity to be associated with the nonlinear processes (such as mode competition and self-induced background plasma modification) as well as the numerous onsets of various parametric processes that occur in regions below the observation height for the HFPL signals. The nonlinear suppression of mode competition on the growth of each spectral line increases with the total spectral intensity

of the excited Langmuir waves, whose linear growth rates increase and angular distribution broadens with the increase of the HF heating power; consequently, the saturation level of the spectral intensity of the down-going HFPL decreases after the HF heating power exceeds the level at time (B). At the onset of a particular parametric instability at a lower height, a larger fraction of the HF power is absorbed and therefore not available for the excitation of the PDI-line signals at the upper height, causing a variation of the nonlinear suppression on the down-going HFPL. From the linear relation of transmitted HF power with time, we may use the time (A) to get the associated HF transmitted power at that time. This power value may then be used to compute the free-space electric field at the range ( $\sim 200$ -km altitude) of interest in units of mV/m for the circularly polarized transmitted HF wave. For this particular time, a value of 53 mV/m was obtained. In the lower ionosphere the “O-Mode”, HF wave remains to be right-hand-circular polarization (with respect to  $B$ ); but it converts to a linear polarization in the region a few km below the HF reflection height, because the radar signals originate from the Langmuir PDI that occurs below, and very close to the HF reflection height, where the HF wave is, in fact, linearly polarized with electric field parallel to the earth’s magnetic field ( $B$ ). Therefore, the free-space circular polarized electric field is enhanced by  $\sqrt{2}$  to give the linear-polarized HF dipole pump field of 75 mV/m. In addition, the field intensity is enhanced by the “swelling” effect. As the HF wave approaches the reflection height, the wave field intensity increases to response to the decrease of the wave group velocity. For vertically incident HF heater, the magnitude of this swelling effect together with the cutoff reflection factor ( $\sim 2$ ) has been estimated to be about a factor of 4 [9], which though decreases with the increase of the oblique incident angle. At  $14^\circ$  incident angle, the swelling factor is reduced to  $4 \times \sin^2 76^\circ \sim 3.76$ . With these two factors (3.76 and  $\sqrt{2}$ ), the experimentally determined threshold field is 281 mV/m. By comparison, the independent theoretical determination by Kuo [10] is 258 mV/m. We consider this to be a very good agreement; a small unknown value of ionospheric absorption would possibly suggest an even more favorable comparison.

It is significant that the experimental results for the L-PDI at HAARP differ from other lower power facilities. Typical results for lower power facilities show the L-PDI decay of the HF wave to an ion-acoustic wave and Langmuir wave [2]. The Langmuir wave from the L-PDI typically has sufficient power to decay into Langmuir and ion-acoustic waves via the “electron decay instability.” This additional Langmuir wave then successively decays in a series of new Langmuir waves termed the “Langmuir cascade.” This Langmuir cascade was also observed at HAARP during the construction phase when only a quarter of the array was operational and was reported by Oyama *et al.* [1] where up to five or six cascade steps were commonly observed. In contrast, after HAARP was completed with full power, the Langmuir cascade was still often observed but limited to one or possibly two cascade steps. This suggests that the power of the Langmuir wave generated by the L-PDI is weaker for HAARP when operating at full power and this is also evident from data in Fig. 1 that show power in the PDI

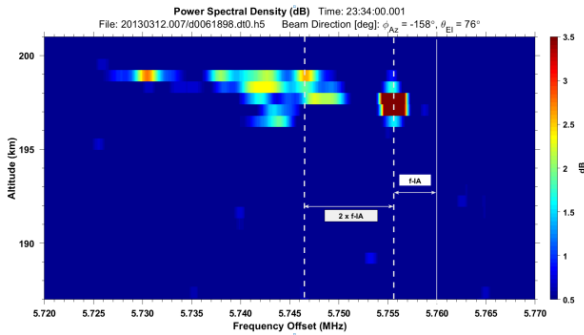


Fig. 3. Doppler power spectra obtained at 2334:00 UT, corresponding to the time marked (B) in Figs. 1 and 2. Vertical range steps are 600 m. The relative power scale was chosen to illustrate the multitude of down-shifted features of the radar signal origin. The HF frequency  $f_0 = 5.760$  MHz is marked as the solid vertical line. The vertical-dashed line near the 5.755 MHz corresponds to the strong PDI line with power that exceeds 10 dB. This is displaced from the HF frequency by about 4.5 kHz (ion-acoustic frequency  $f_i$ ). The other dashed line located 9 kHz to the left is shifted by  $3f_i$  from  $f_0$  and is the expected excitation location of the first cascade line.

line (relative power of the Langmuir wave that results from the L-PDI) drops when other processes at lower heights take place. Furthermore, in Fig. 4, it is evident that during artificial ionization, the Langmuir cascade is completely absent. The L-PDI operates just below the HF cutoff height and is associated with O-mode linear polarization. The HAARP facility has sufficient power to exceed the threshold for numerous other parametric processes and creation of artificial ionization that occur at lower heights where the HF O-mode wave is circularly polarized and not evolved to linear polarization at upper heights; it effectively extracts power from the HF wave before it reaches the height where the L-PDI operates. As a result, there is minimal HF power available at the upper height just below the HF cutoff frequency where the L-PDI operates. In addition, as discussed earlier, we also suggest that nonlinear suppression of mode competition [15] which increases with the higher HF power is also a factor.

It is of interest to note that Bryers *et al.* [11] used a different approach with the EISCAT facility to estimate the threshold field for the L-PDI from ion-line signals and stepped the HF power over five values. They estimated the threshold field to be about 0.25 V/m that is close to the value determined for HAARP.

Fig. 3 shows the HFPLs power spectra as a function of height at time (B) when the spectral intensity of the down-going PDI-line peaks. It is of interest to note that many down-shifted signals appear at this time and are rapidly varying in frequency and power. These likely result from the startup of various unknown parametric processes. It is also notable that there is no clear evidence of the cascade lines in the HFPLs that are observable at other low-power facilities. The dashed line drawn near 5.746 may possibly indicate evidence for the first cascade line of the up-going PDI line; it occurs about 1 km above the PDI-line height. However, it is very transient in nature.

Returning to Fig. 2, the time (C) marks the approximate time when the height of the radar signals begins to drop due to the

start of artificial ionization. From this figure, the exact time for the onset of this process is unclear and we have, therefore, developed an alternative method using the PDI-line power that clearly determines the onset time with less than 500-ms uncertainty. Referring to Fig. 1, the time (C) that corresponds to a peak in the PDI-line power occurs when the height of the radar returns in Fig. 2 starts to drop. We, therefore, identify this peak to be the onset time of the parametric process responsible for artificial ionization. The PDI-line relative power drops after this time because available power is diverted to the ionization production process and less power available at upper levels where the PDI line is observed.

Individual power spectra were manually examined in a similar manner to that described previously for determining time A. The peak in the relative power of the PDI line at time C marked in Fig. 1 was determined to be 2334:43.0 UT, i.e.,  $t = 103.0$  s used to calculate the EIRP to be 86.05 dBW (EIRP  $\sim 403$  MW). The corresponding electric field value at 200-km height is 550 mV/m. The spectral analysis was conducted with 500ms integration periods and used to determine time of the peak returned PDI signal power. This time was unambiguous and corresponded to only one integration period. Since each time step of 500ms corresponds to about 10mV/m of computed freespace electric field, we therefore suggest any uncertainty in selecting this time introduces a maximum uncertainty of about 10mV/m for the computed field value. This is the free-space field for the right-hand circular polarized wave that occurs near the upper-hybrid resonance height. Unlike the PDI discussed earlier, there is no “swelling” effect. The condition for the plasma frequency  $\omega_p$  at the matching height for minimum threshold  $E$ -field for this upper-hybrid PDI process [10], [12] is  $\omega_p = (\omega_o^2 - \Omega_e^2 - 3k^2v_{te}^2) < (\omega_o^2 - \Omega_e^2)^{1/2}$  where  $\omega_o$  is the HF heater frequency,  $\Omega_e$  is the electron gyro-frequency, and  $v_{te}$  is the electron thermal speed. Since  $(\omega_o^2 - \Omega_e^2)^{1/2}$  is the plasma frequency of the upper-hybrid resonance layer, this implies that the minimum threshold field occurs below the height of the upper-hybrid resonance. The EIRP of about 403 MW is significantly less than the maximum full power value of 1.6 GW that is available for the HF frequency used in this experiment. This is consistent with other experiments at HAARP where artificial ionization was observed with radiated powers 25%–50% of the full power value.

It is notable that the PDI-line frequency that is down-shifted about 4.5 kHz from the HF value remains close to this value during HF power increase with very small variations. This down-shifted frequency is temperature-dependent and proportional to the ion-acoustic speed  $C_s = [(T_e + 3T_i)/m_i]^{1/2}$ . No significant increases of the down-shifted value of the PDI line were observed as the HF power was increased. It is noted that HF heating mainly acts on the electron plasma; on the other hand, the ion-acoustic speed is more sensitive to the ion temperature change, for example, for  $T_i = 2/3T_{e0}$ , 100% electron temperature elevation, i.e.,  $T_e = 2T_{e0}$ , only increases ion acoustic frequency by about 15%. Moreover, the field-aligned thermal conduction acts to suppress local electron heating near the HFPLs height because heat is rapidly conducted to the upper ionosphere. This is consistent

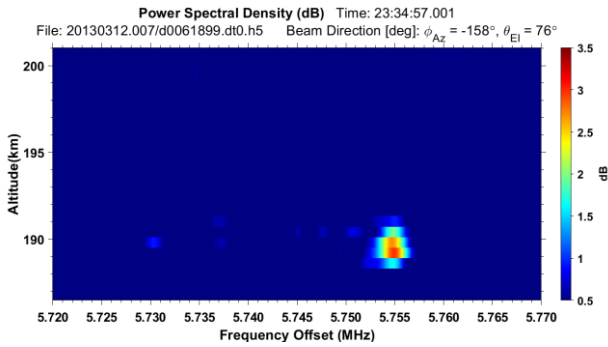


Fig. 4. Power spectra at a time during the period of artificial ionization production. The strongest signals at 5.755 MHz are the PDI line measured with the UHF diagnostic radar. The HF frequency transmitted by HAARP was 5.760 MHz.

with other observations. For example, Rietveld *et al.* [13] at the EISCAT facility found significant  $T_e$  increases at upper  $F$ -region heights from 300 to 600 km (the highest level measured) and upward ion-flow. Furthermore, Fallen *et al.* [14] found experimental evidence from *in situ* observations at 900 km above HAARP for field-aligned upward plasma fluxes that are likely temperature-driven enhanced ambipolar flow.

Fig. 4 shows the power spectra at 23:34:53 UT during the production of artificial ionization; at this time, the height of the PDI-line signals is descending. As ionization is produced, the increasing density causes the HF interaction to occur at successively lower heights. In addition to the PDI-line signals at 5.755 MHz there is evidence of very weak down-shifted signals to 5.730 MHz, the origin of these is likely the linear mode conversion of the down-going upper-hybrid waves which are excited by the upper-hybrid PDI with the lower-hybrid decay mode. The power in the PDI line is quite weak compared with earlier times with lower HF radiated power and there is no evidence of a Langmuir cascade spectrum in the HFPLs, presumably mainly due to the nonlinear suppression of mode competition [15] which increases with the increase of the HF power.

### III. SUMMARY

An experiment at HAARP was conducted at the HF frequency of 5.760 MHz where the HF heating power in EIRP was increased from 100 kW to 1.6 GW over a 2-min period. The HF frequency was initially about 2–5 kHz above the computed fourth electron gyro-harmonic frequency. A UHF diagnostic radar was used to determine the onset time of the HFPLs and, hence, EIRP at this initial onset time. The HFPLs and other Langmuir waves corresponding to the Langmuir PDI, which decays the high-power HF pump wave to Langmuir sidebands and ion-acoustic decay modes, are excited below and close to the HF reflection height. The EIRP (about 3.8 MW) of the HF heater, which radiated at RH circular polarization along the magnetic zenith, was then used to calculate the free-space circular-polarized electric field at the range of interest and found to be 53 mV/m. After accounting for the linear dipole pump conversion ( $\sqrt{2}$ ), and swelling effect (about a factor of 3.76) close to the HF reflection height where the PDI process occurs, we obtain a value of 281 mV/m that is in very good agreement with an independent estimate

of 258 mV/m from theory. A small unknown absorption of the HF wave in the lower ionosphere would possibly bring the experiment and theory values even closer.

Subsequently, due to ionization production, the HF interaction height dropped by about 10 km when the HF heater was turned off and at that end time, the HF frequency was about 10 kHz below the local gyro-harmonic value. Similar to many other examples, further ionization production down to about 150-km height would have occurred if the HF power had remained on for a longer time.

The onset of artificial ionization may be recognized from the downward progression of the Langmuir sidebands observed by the diagnostic radar; however, there is considerable uncertainty in determining the onset time from the power-time-height data. We have developed an alternative approach that establishes the onset time for ionization production with about 1-s uncertainty. This is done through spectral analysis and monitoring the spectral power in the PDI line only.

The peak in the PDI-line power evolution (near the starting time of the downward trend of the total scattered power) is used as the indicator to identify the spectral onset time. The HF EIRP at this time is then adopted to calculate the HF electric field in the upper-hybrid resonance region, where the HF heater remains to be RH-circular polarization. With EIRP = 403 MW, the free-space HF field is obtained to be about 550 mV/m.

For HAARP, the threshold field of the upper-hybrid PDI, presented in [10, Eq. (7.31)] with the adjustment on the HF frequency from 5 to 5.76 MHz (see 7.27), is given to be  $E_{th} \sim 0.54\xi^{1/2}\lambda^2\{1 + 0.87 \times 10^5[\xi/(\xi-1)]^{1/2}\}\lambda^3 \exp[-43.56\lambda^2\xi/(\xi-1)]^{1/2}$ .

The lower-hybrid resonance frequency is  $f_{LH} \sim (f_{ce}f_{ci})^{1/2} \sim 8.16$  kHz. The down-shifted signals of 5.73 MHz in Fig. 4 suggest that lower-hybrid decay mode in the upper-hybrid PDI has a frequency  $f_L \sim 30$  kHz =  $f_{LH}\xi^{1/2}$ , where  $\xi = 1 + (m_i/m_e)(k_z^2/k_\perp^2)k_z$  and  $k_\perp$  are the parallel and perpendicular (to the geomagnetic field) components of the lower-hybrid wave vector. Therefore,  $E_{th} = 550$  mV/m corresponds to  $\lambda \sim 0.53$  m, which is indeed in the wavelength regime of large growth rate. Short wavelength upper-hybrid waves implement Doppler shifted harmonic-cyclotron resonance interaction, via finite Larmor radius effect, to effectively accelerate electrons [16]. Artificial ionization by the accelerated electrons in the lower region was detectable via UHF radar.

These results apply to the particular case where the initial HF frequency was selected for the reflection height close to the fourth electron gyro-harmonic. Operating with an HF interaction height significantly above or below this level may yield different results.

### REFERENCES

- [1] S. Oyama, B. J. Watkins, F. T. Djuth, M. J. Kosch, P. A. Bernhardt, and C. J. Heinselman, "Persistent enhancement of the HF pump-induced plasma line measured with a UHF diagnostic radar at HAARP," *J. Geophys. Res.*, vol. 111, no. A6, 2006, Art. no. A06309, doi: [10.1029/2005JA011363](https://doi.org/10.1029/2005JA011363).
- [2] D. B. Muldrew and R. L. Showen, "Height of the HF-enhanced plasma line at arcicob," *J. Geophys. Res.*, vol. 82, no. 29, pp. 4793–4804, Oct. 1977.

- [3] P. Stubbe, "The ionosphere as a plasma laboratory," in *Modern Ionospheric Science*, K. Schlegel, H. Kohl, and R. Ruste, Eds. Katlenburg-Lindau, Germany: European Geophysical Society, 1996.
- [4] T. Pedersen *et al.*, "Optical ring formation and ionization production in high-power HF heating experiments at HAARP," *Geophys. Res. Lett.*, vol. 36, no. 18, 2009, Art. no. L18107, doi: [10.1029/2009GL040047](https://doi.org/10.1029/2009GL040047).
- [5] E. Mishin, B. Watkins, N. Lehtinen, B. Eliasson, T. Pedersen, and S. Grach, "Artificial ionospheric layers driven by high-frequency radiowaves: An assessment," *J. Geophys. Res., Space Phys.*, vol. 121, no. 4, pp. 3497–3524, Apr. 2016, doi: [10.1002/2015JA021823](https://doi.org/10.1002/2015JA021823).
- [6] L. Stenflo, "Parametric excitation of collisional modes in the high-latitude ionosphere," *J. Geophys. Res.*, vol. 90, no. A6, p. 5355, 1985.
- [7] S. P. Kuo, "Ionospheric modifications in high frequency heating experiments," *Phys. Plasmas*, vol. 22, no. 1, Jan. 2015, Art. no. 012901, doi: [10.1063/1.4905519](https://doi.org/10.1063/1.4905519).
- [8] B. Watkins, S. Kuo, J. Secan, and C. Fallen, "Ionospheric HF heating experiment with frequency ramping-up sweep: Approach for artificial ionization layer generation," *J. Geophys. Res., Space Phys.*, vol. 125, no. 3, Mar. 2020, doi: [10.1029/2019JA027669](https://doi.org/10.1029/2019JA027669).
- [9] S. P. Kuo, "Cascade spectrum of HF enhanced plasma lines generated in HF heating experiments," *J. Geophys. Res.*, vol. 110, no. A1, 2005, Art. no. A01309.
- [10] S. Kuo, *Plasma Physics in Active Wave Ionosphere Interaction*. Singapore: World Scientific, 2018.
- [11] C. J. Bryers, M. J. Kosch, A. Senior, M. T. Rietveld, and T. K. Yeoman, "The thresholds of ionospheric plasma instabilities pumped by high-frequency radio waves at EISCAT," *J. Geophys. Res. Space Phys.*, vol. 118, no. 11, pp. 7472–7481, 2013, doi: [10.1002/2013JA01929](https://doi.org/10.1002/2013JA01929).
- [12] S. Kuo and A. Snyder, "Artificial plasma cusp generated by upper hybrid instabilities in HF heating experiments at HAARP," *J. Geophys. Res., Space Phys.*, vol. 118, no. 5, pp. 2734–2743, May 2013, doi: [10.1002/jgra.50276](https://doi.org/10.1002/jgra.50276).
- [13] M. T. Rietveld, M. J. Kosch, N. F. Blagoveshchenskaya, V. A. Komienko, T. B. Leyser, and T. K. Yeoman, "Ionospheric electron heating, optical emissions, and striations induced by powerful HF radio waves at high latitudes: Aspect angle dependence," *J. Geophys. Res.*, vol. 108, no. A4, pp. 1141–1156, 2003, doi: [10.1029/2002JA009543](https://doi.org/10.1029/2002JA009543).
- [14] C. T. Fallen, J. A. Secan, and B. J. Watkins, "In-situ measurements of topside ionosphere electron density enhancements during an HF-modification experiment," *Geophys. Res. Lett.*, vol. 38, no. 8, Apr. 2011, Art. no. L08101, doi: [10.1029/2011GL046887](https://doi.org/10.1029/2011GL046887).
- [15] S. P. Kuo, M. C. Lee, and F. T. Djuth, "A new interpretation of plasma-line overshoot phenomena," *Geophys. Res. Lett.*, vol. 14, no. 9, pp. 961–964, Sep. 1987.
- [16] S. P. Kuo, "Electron cyclotron harmonic resonances in high-frequency heating of the ionosphere," *Phys. Plasmas*, vol. 20, no. 9, Sep. 2013, Art. no. 092124, doi: [10.1063/1.4822336](https://doi.org/10.1063/1.4822336).
- [17] K. Davies *Ionospheric Radio Waves*. London, U.K.: Blaisdel Publishing, 1969.



**Brenton J. Watkins** (Member, IEEE) received the B.Sc. degree in mathematics and physics from The University of Adelaide, Adelaide, SA, Australia, in 1968, the M.S. degree in physics from La Trobe University, Melbourne, VIC, Australia, in 1972, and the Ph.D. degree in physics from the University of Alaska Fairbanks, Fairbanks, AK, USA, in 1976.

He was a Physics Department Member with the University of Alaska Fairbanks from 1980 to 2011 and taught a number of physics and computer science classes where he served as the Department Chair. In 1981, he was a Summer Faculty Research Fellow with the Air Force Research Laboratory, Hanscom Air Force Base, Lincoln, MA, USA. He was a Visiting Professor with Nagoya University, Nagoya, Japan, in 2008 and 2013. He also held earlier research positions at the MIT Lincoln Laboratory, Lexington, MA, USA, and North-East Radio Observatory Corporation, Westford, MA, USA, La Trobe University, and the Australian Antarctic Research Program. He is currently an Emeritus Professor of physics with the University of Alaska Fairbanks. His research activities have focused on many aspects of atmospheric and space science, including ionospheric observations using incoherent-scatter radar, development of radar techniques to detect turbulence in the troposphere and stratosphere, laser and microwave propagation through atmospheric turbulence, numerical modeling of the ionosphere, radar detection of metallic ions in the upper atmosphere, and modeling and wave-tracing analysis of radar wave propagation through the atmosphere and ionosphere for the prediction of target errors in defense radars. His current research interests include ionospheric modification using high-power HF radio waves and associated wave-plasma interactions.



**Spencer P. Kuo** (Fellow, IEEE) received the B.S. and M.S. degrees from National Chiao Tung University (NCTU), Hsinchu, Taiwan, in 1970 and 1973, respectively, and the Ph.D. degree from the Polytechnic Institute of New York, New York, NY, USA, in 1977.

Since 1986, he has been a Full Professor with the Electrical and Computer Engineering Department, Polytechnic University (now New York University Tandon School of Engineering), New York, where he initiated and ran a Summer Research Program for College Juniors from 1985 to 1991. This program, which has gained nationwide popularity, has since been adopted in many universities and national laboratories. He published two books, more than 200 journal articles, and 87 proceedings issued articles. He holds six U.S. patents and four foreign patents. Under his supervision, 14 students received doctorates. His current research interests include microwave-plasma interactions, waves in the ionosphere and magnetosphere, plasma torches, plasma mitigation of shock waves, and plasma for industrial and medical applications.

Dr. Kuo received the Outstanding Research Award from the Scientific Research Society Sigma Xi in 1990. The Chinese Institute of Engineers (CIE), USA, named him the 2005 Asian-American Engineer of the Year. He was honored with the Distinguished Alumnus of his Alma Mater, NCTU, in 2013.